Quaternary Science Reviews 126 (2015) 227–241

Contents lists available at ScienceDirect

Quaternary Science Reviews

journal homepage: www.elsevier.com/locate/quascirev

A multi-proxy reconstruction of environmental change spanning the last 37,000 years from Burial Lake, Arctic Alaska

M.S. Finkenbinder [a, *], M.B. Abbott [a], B.P. Finney [b, c], J.S. Stoner [d], J.M. Dorfman [d]

[a] Department of Geology and Planetary Science, University of Pittsburgh, Pittsburgh, PA, USA
[b] Department of Biological Sciences, Idaho State University, Pocatello, ID, USA
[c] Department of Geosciences, Idaho State University, Pocatello, ID, USA
[d] College of Earth, Ocean, and Atmospheric Sciences, Oregon State University, Corvallis, OR, USA

ARTICLE INFO

Article history:
Received 7 January 2015
Received in revised form
25 August 2015
Accepted 31 August 2015
Available online xxx

Keywords:
Alaska
Eastern Beringia
Late-Quaternary
Last Glacial Maximum
Holocene
Climate change
Biogenic silica
Magnetic susceptibility
Carbon and nitrogen isotopes
Scanning X-ray fluorescence

ABSTRACT

Sediment cores from Burial Lake located in the western Brooks Range in Arctic Alaska record paleoenvironmental changes that span the last 37,000 calendar years before present (cal yr BP). We identified four distinct lithologic subunits based on physical properties (dry bulk density, magnetic susceptibility), sediment composition, and geochemical proxies (organic matter, biogenic silica, C/N, organic matter $\delta^{13}C$ and $\delta^{15}N$, and elemental data from scanning X-ray fluorescence). The multi-proxy approach and relatively high temporal resolution (at multi-decadal to centennial time scales) of our proxy analysis, compared with previous studies of intermediate water depth cores from Burial Lake, provide new insights into the paleoenvironmental history of the region spanning the period prior to the Last Glacial Maximum. Relatively high lake-levels and gradually decreasing in-lake and terrestrial productivity occur during the mid-Wisconsin interstadial from 37,200 to 29,600 cal yr BP. The subsequent period is defined by falling and lower lake-levels with decreasing effective-moisture, windier conditions, and sustained low aquatic productivity throughout the LGM between 29,600 and 19,600 cal yr BP. The last deglaciation that commenced by 19,600 cal yr BP is characterized by gradual changes in several sediment physical and geochemical proxies, including increasing C/N ratios and terrestrial productivity, decreasing magnetic susceptibility and clastic sediment flux, along with rising and relatively higher lake-levels. A decrease in aeolian activity after 16,500 cal yr BP is inferred from the appearance of fine (very fine sandy silt) sediment, compared to coarse sediments through the LGM and last deglaciation. The highest levels of terrestrial inputs along with increasing and variable aquatic productivity occur during the Lateglacial to early Holocene interval between 16,500 and 8800 cal yr BP. The absence of multi-proxy evidence for a strong climatic reversal during the Younger Dryas from Burial Lake sediments contrasts with some paleorecords showing cooler temperatures and/or dry conditions in northern Alaska at this time. Peak levels of sediment organic content and terrestrial productivity at Burial Lake between 10,500 and 9900 cal yr BP coincide with the early Holocene summer insolation maxima, which likely represents summertime warming and an enhanced flux of watershed derived organic matter from permafrost degradation. The remainder of the Holocene (since 8800 cal yr BP) at Burial Lake is characterized by relatively high and stable lake levels, landscape stabilization, and relatively high and variable levels of aquatic productivity.

1. Introduction

Recent climate change in the Alaskan Arctic is a having a profound effect on aquatic and terrestrial ecosystems, the surface hydrology of lakes and ponds, and the stability of permafrost landscapes. For example, warming temperatures between A.D. 1990 and 2009 coincide with an increase in the abundance of shrubs and terrestrial productivity in tundra landscapes across Arctic Alaska (Swanson, 2010). Accelerated permafrost degradation and thaw slumping observed in the Noatak Basin have been attributed to general climate warming and shifting trends in the seasonality of weather (Balser et al., 2014). Further, an ~30% decrease in pond and

* Corresponding author.
E-mail address: msf34@pitt.edu (M.S. Finkenbinder).

http://dx.doi.org/10.1016/j.quascirev.2015.08.031
0277-3791/

thaw lake surface area on the Alaskan North Slope between A.D. 1948 and 2013 corresponded with increases in air temperature and permafrost active layer thickness (Andresen and Lougheed, 2015). The drying and disappearance of these tundra ponds near Barrow, Alaska has been linked with increased evaporation from warming, permafrost degradation, and increased emergent vegetation. Additional changes include a decrease in lake ice cover duration by 24 days between A.D. 1950 and 2011 on the Alaskan North Slope (Surdu et al., 2014) and shrinking sea-ice cover in the adjacent Chukchi Sea (Wendler et al., 2014). Understanding the significance of these terrestrial ecosystem changes and of natural climate variability in the Alaskan Arctic requires a longer-term perspective than is provided by instrumental weather records and satellite observations, so that they might be placed in an appropriate context.

The late-Quaternary climatic and environmental history of the Arctic Noatak Basin in the western Brooks Range in Alaska, confined by the Delong Mountains to the north and Baird Mountains to the south, is primarily based on extensive surficial mapping and analysis of alluvial, lacustrine, and glacial deposits (Hamilton and Van Etten, 1984; Hamilton et al., 1987; Hamilton, 2001, 2010). Alluvial deposits along Noatak River and tributaries show extensive aggradation during stadial periods and channel incision, floodplain construction, and soil formation during interstadial periods (Hamilton, 2010). Glaciolacustrine and ice-contact glacial deposits are scattered throughout the basin and provide evidence for large proglacial lakes and periods of moraine construction spanning the middle Pleistocene to the Last Glacial Maximum (LGM) or late Wisconsin (Hamilton and Van Etten, 1984; Hamilton et al., 1987). For instance, bracketing radiocarbon ages constrain the LGM to between 35 and 13.6 ka ^{14}C years in the western Noatak Basin (Hamilton, 2010). Floodplain aggradation on Noatak River ended by or shortly after 13.6 ka ^{14}C years and was followed by Holocene channel incision and down-cutting (Hamilton, 2001). Further evidence for climatic and environmental changes in the Noatak Basin are inferred from palynological analysis of sediment cores from several lakes including Kaiyak (Anderson, 1985), Niliq (Anderson, 1988), and Feniak (Eisner and Colinvaux, 1992) (all shown in Fig. 1) along with analysis of fossil beetle assemblages to interpret temperatures (Elias et al., 1999; Elias, 2000). More recently, core-transect and multi-proxy analysis (pollen, organic geochemical proxies, and chironomids) of intermediate water depth (7.9 m) cores from Burial Lake (Fig. 1) reconstructed changes in relative lake-levels, vegetational patterns, and summer temperatures across the last 40,000 years (Kurek et al., 2009; Abbott et al., 2010), however, an unconformity and missing sediments spanning the LGM limited the scope of these studies. Collectively, the previous studies and environmental interpretations are limited by the complex and discontinuous nature of surficial stratigraphic deposits (Elias, 2000; Hamilton, 2001), bulk sediment radiocarbon dating and emphasis on pollen analysis to assess environmental changes (Anderson, 1985, 1988; Eisner and Colinvaux, 1992), and the coarse resolution of proxy analysis and missing sediments through the LGM (Kurek et al., 2009; Abbott et al., 2010).

The primary objective of this study was to investigate climatic and environmental changes from the interstadial period prior to the LGM to the present from multi-proxy analysis of newly recovered Burial Lake depocenter cores (21.5 m water depth). In this study, we analyzed multiple physical and geochemical proxies (including dry bulk density, organic matter, biogenic silica, carbon to nitrogen mass ratios (C/N), stable carbon and nitrogen isotopes (δ^{13}C and δ^{15}N) of organic matter, and elemental abundances via scanning X-ray fluorescence) along with sediment description and used Accelerator Mass Spectrometry (AMS) radiocarbon dating of wood, seeds, and plant macrofossils to establish age control. Proxies in this study were analyzed at much higher temporal resolution than previous works at Burial Lake to investigate multi-decadal to century scale variations in environmental conditions. Comparison with a newly developed environmental magnetic record from the same sediment cores (Dorfman et al., in this issue), other regional glacial and lacustrine records from northwest Alaska, along with nearby marine records provides an assessment and new synthesis of regional climatic change in the western Brooks Range during the late Quaternary.

2. Site location and regional setting

Burial Lake (68.43°N, 159.17°W; 460 m ASL) is located in the upper Anisak River drainage within the Noatak Basin in the northwestern Brooks Range, Alaska (Fig. 1). The surface area of Burial Lake is approximately circular (0.8 km^2) and has a maximum water depth of 21.5 m. The lake is situated on a subtle topographic high between Setting Sun Creek to the west and a small tributary to the east (Fig. 1) that drains to Anisak River and eventually Noatak River. The surrounding catchment is small (3.3 km^2) with steep (3–5 m high) slopes along much of the lake's shoreline that transition to a low-relief plateau. The lake receives inflow from several ephemeral gullies along the northern shoreline and contains a small outlet stream at the southwest shoreline. Burial Lake is oligotrophic and a hydrologically open system. Vegetation is low-arctic tundra, dominated by sedges, *Salix*, shrub-*Betula*, and *Alnus crispa*, with sparse stands of *Populus balsamifera* found in river valleys and along creek beds (Abbott et al., 2010). Tree-line for the nearest *Picea glauca* (spruce) forest lies ~100 km to the west, and also encroaches on the Basin from the south.

The lake is located in the Aniuk Lowland sub-province within the Noatak Lowland physiographic province, an irregular rolling plain that slopes gradually to the south (Wahrhaftig, 1965). The Delong Mountains flank the lake and catchment to the north and consist of a series of rugged glaciated ridges with altitudes >1250 m, while the lower altitude (>900 m) Iggiruk Mountains are located to the south. Bedrock geology in the catchment consists of Mississippian age carbonate and clastic sedimentary rocks, consisting of limestone and subordinate shale, chert, and dolomite (Grybeck et al., 1977). Surficial geology in the catchment is mapped as Itkillik I age (early Wisconsin, Marine Isotope Stage 4) lake deposits, Holocene to late Pleistocene age solifluction deposits, and silt-covered (loess) bedrock (Hamilton, 2010). The catchment and surrounding region is underlain by continuous permafrost and ground ice is mapped as low or <10% volume (Jorgenson et al., 2008). During the Sagavanirktok River glaciation (middle Pleistocene age), alpine glaciers originating in the Delong Mountains scoured the landscape and dammed local drainage, forming the lake basin (Hamilton, 2003a). Subsequent glacier advances in the Noatak Basin were less extensive, including during early Wisconsin (Itkillik I) and late Wisconsin (Itkillik II) advances (Hamilton, 2001), and glaciers did not extend across the lake and adjacent terrain during the LGM. During middle and late Pleistocene glacial periods, alpine glaciers emanating from the Delong Mountains extended into the lowlands and repeatedly dammed Noatak River forming Glacial Lake Noatak (Hamilton and Van Etten, 1984). While the lake was not covered by Itkillik II age (LGM) lacustrine deposits, the lower Anisak River valley and western Noatak Basin were inundated by Glacial Lake Noatak (Hamilton, 2010). During the LGM, alpine glacial erosion resulted in outwash deposition and extensive floodplain aggradation in the Noatak Basin (Hamilton, 2001).

The regional climate in the Noatak Basin is characterized by long cold winters and short cool summers. Bieniek et al. (2012) place the upper Noatak Basin within the North Slope climate division, a region defined by arid conditions (maximum precipitation of <5 cm in the wettest summer month) with seasonal average temperatures

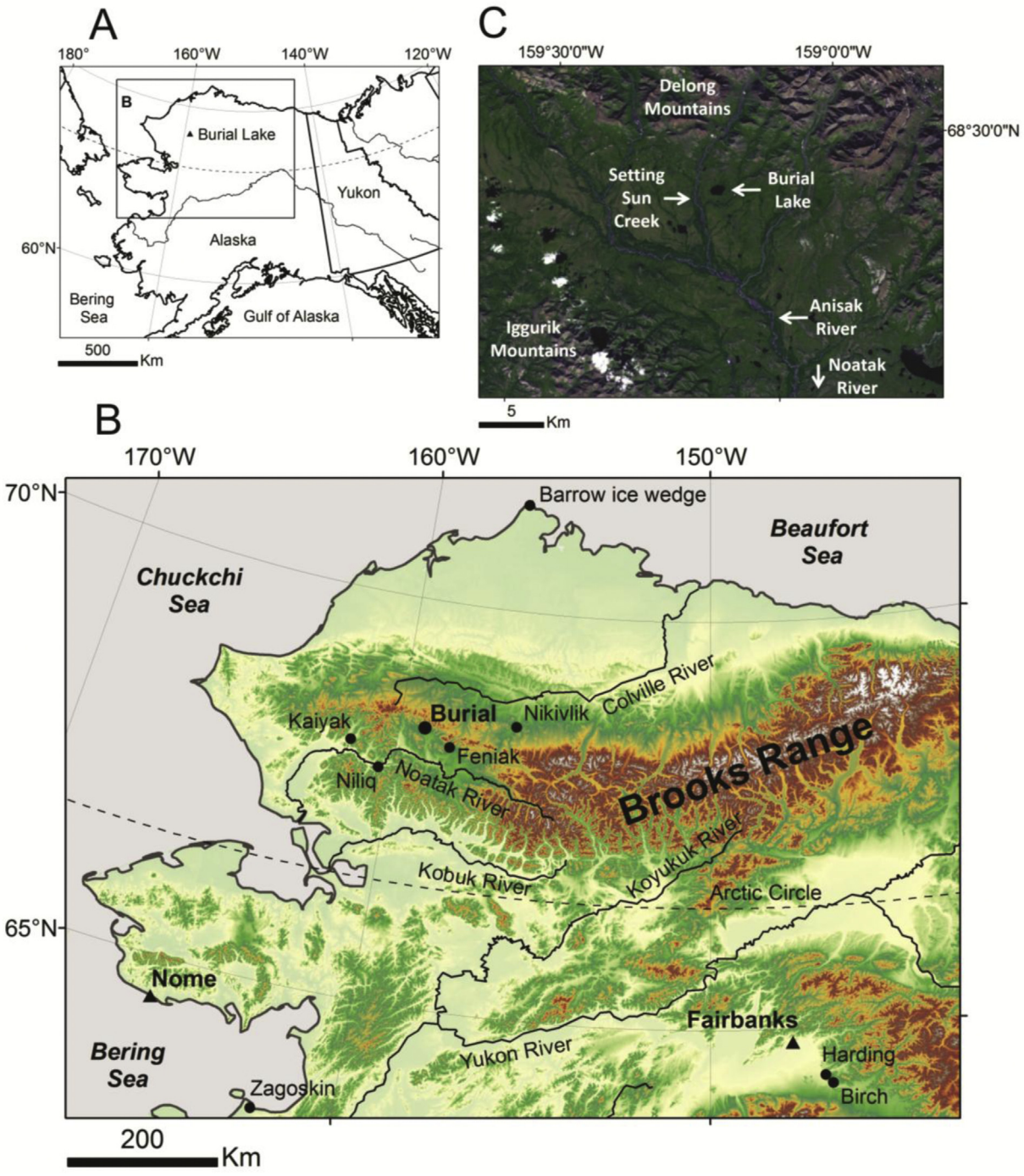

Fig. 1. A) Regional map of Alaska showing the location of Burial Lake. B) Shaded relief map of the western Brooks Range in Alaska with sites mentioned in the text. Solid lines are major rivers. C) Aerial photograph of the Upper Anisak River drainage showing Burial Lake and the surrounding area.

ranging from below −25 °C in winter to above 10 °C in summer. Instrumental weather records from the Noatak Basin are relatively short and discontinuous. Climate normals for stations across northern Alaska (Kotzebue, Bettles, and Barrow) during the period 1981–2010 indicate the majority of annual precipitation occurs during summer months, with peak values typically occurring in July and August (http://climate.gi.alaska.edu/). Summer precipitation to the interior of Alaska is primarily sourced from the North Pacific Ocean (Streten, 1974; Mock et al., 1998). Climatic conditions in northern Alaska are further influenced by ocean–atmosphere interactions and internal modes of climate variability (El Niño Southern Oscillation, Pacific Decadal Oscillation, and Arctic Oscillation) on seasonal to multi-decadal timescales (Papineau, 2001; Hartman and Wendler, 2005; Bieniek et al., 2012).

3. Methods

3.1. Sediment coring

Sediment cores were collected from an inflatable raft from the

central deep basin in July, 2010 (Fig. 1C). A surface core (A-10 Drive 1) with an intact sediment–water interface was recovered from 21.5 m water depth using a polycarbonate tube fit with a rubber piston. The upper portion of the surface core was dense and therefore packed with floral foam and capped for transport. Multiple overlapping long cores were recovered from core sites A-10 and C-10 in 21.5 m water using a square rod Livingstone corer. Deeper sediments, characterized by greater density, were recovered by coring within the same borehole using 10 cm diameter PVC as casing. Cased drives were offset by 50 cm between core sites A-10 and C-10 to ensure overlap and complete recovery of the sediment sequence.

3.2. Lithostratigraphy and geochemistry

Sediment cores were split lengthwise and described; notable sedimentary structures, grain size, and Munsell color were characterized for each core. Select 1 cm samples spanning the composite depth scale were analyzed and described via smear-slide mineralogy (Schnurrenberger et al., 2003). A total of 5 samples were analyzed for powder X-ray diffraction (XRD) to further characterize core mineralogy. Power XRD analysis was performed using a using a Philips PW3710 X-ray diffractometer at the University of Pittsburgh, Swanson School of Engineering and X'Pert Graphics and Identify® software was used to identify the major mineral assemblages present. All cores were sampled at 1 cm intervals, and dry bulk density was calculated from dry weights of volumetric samples, and percent organic matter and total carbonate values were measured via loss-on-ignition (LOI) at 550 °C for 4 h and 1000 °C for 2 h, respectively (Heiri et al., 2001). Magnetic susceptibility was measured on all split cores at 2 mm intervals using a Bartington MS2E1 high-resolution surface sensor.

Samples for biogenic silica were measured at 2–4 cm intervals over the composite core (n = 256) at the Department of Geology and Planetary Science at the University of Pittsburgh using a wet-chemistry, alkaline extraction adapted from Mortlock and Froelich (1989). Wet samples were freeze-dried, homogenized to a fine powder using a mortar and pestle, and treated with 30% H_2O_2 and 1 M HCl to remove organic matter and carbonates. Biogenic silica was extracted with a 5% Na_2CO_3 solution and determined by molybdate blue spectrophotometry at 812 nm using a Thermo Scientific Evolution 60s UV–Visible Spectrophotometer. Replicate measurements of unknown samples (n = 44) and an internal sediment standard from Laguna de Los Anteojos (Stansell et al., 2010) run during sample analysis produced an average error of <3.2%.

Samples for total organic carbon (TOC), total nitrogen (TN), and stable carbon ($\delta^{13}C$) and nitrogen ($\delta^{15}N$) isotopes of organic matter were measured at 2–4 cm intervals over the composite core (n = 222) at the Stable Isotope Laboratory at Idaho State University. Prior to analysis, samples were treated with 1 M HCl, rinsed to neutral pH with MilliQ water, freeze-dried and homogenized. Measurements were obtained using an Elemental Combustion System 4010 interfaced to a Delta V Advantage mass spectrometer through the ConFlo IV system. $\delta^{13}C$ and $\delta^{15}N$ values are reported as ‰ values relative to the VPDB and N_2 scales, respectively. Replicate measurements of internal standards yielded coefficients of variation of 1.61% and 1.04% for TOC and TN, and precision equal to 0.2‰ for the stable isotope measurements. Surface water samples from Burial Lake collected in August, 1997 were analyzed for pCO_2 concentrations via the headspace equilibration technique (Kling et al., 1991).

The split A-10 and C-10 archive cores were scanned for elemental abundances using the ITRAX XRF core scanner at the Large Lakes Observatory, University of Minnesota Duluth. Continuous measurements were obtained at 0.5 cm intervals with 60 s count times. Values are reported as counts per second. To assess controls on elemental abundances, we analyze trends in the incoherent to coherent scatting ratio (Inc/Coh) and silicon to titanium (Si/Ti) ratio, two commonly used XRF proxies. The Inc/Coh ratio provides a relative measure of the mean atomic number for elements in a sample and therefore is a useful proxy for total organic matter (Croudace et al., 2006). The Si/Ti ratio is another commonly used proxy to estimate the relative proportion of biogenic silica in lake sediments (Brown et al., 2007) and is based on the premise that titanium is sourced solely from detrital sources, while silicon is derived from both biogenic and detrital sources.

3.3. Chronology

Age control of the recovered material was developed from Accelerator Mass Spectrometry (AMS) radiocarbon analyses of 13 samples of wood, seeds, and plant macrofossils. Bulk sediment samples were disaggregated with dilute H_2O_2 (7%), wet-sieved with a 63 μm sieve, and macrofossils or wood were picked under a stereographic microscope for AMS radiocarbon measurement. The non-woody plant macrofossils displayed clear evidence of vascular structure. Samples were pre-treated using standard acid–base–acid wash techniques (Abbott and Stafford, 1996) at the University of Pittsburgh and were combusted to CO_2 gas, converted to filamentous graphite, pressed in Aluminum targets, and measured at the W.M. Keck Carbon Cycle AMS Laboratory, University of California, Irvine. Radiocarbon ages were calibrated using CALIB 6.0 and the INTCAL09 calibration curve (Reimer et al., 2009). An age–depth model was created using point to point, linear interpolation with the classical age modeling (CLAM) code for the statistical software R (Blaauw, 2010). The CLAM analysis performed 1000 age model iterations based on repeated sampling of the calibrated age distributions for each radiocarbon sample to estimate the ‘best fit’ or weighted mean age for each depth. To further account for chronological uncertainty, given the paucity of materials for dating between 219 cm and 553 cm (Table 1), we apply a Monte Carlo-based approach that perturbs the interpolated age–depth model 10,000 times following a random draw from a normal distribution between the 2σ calibrated ^{14}C ages (Marcott et al., 2013). The uncertainty between the age control points is modeled as a random walk (Huybers and Wunsch, 2004), with chronological uncertainty assumed to be auto-correlated through time and modeled as a first order autoregressive (AR1) process.

4. Results

4.1. Composite core

A composite 651 cm depth scale was developed from cores A-10 and C-10. Cores were aligned by matching physical properties data (magnetic susceptibility and Inc/Coh from scanning XRF) and visible stratigraphic markers common to both cores (Supplemental Fig. 1). Core A-10 was selected as the primary core due to its greater length and abundance of proxy data sets including radiocarbon samples. The A-10 core stratigraphic section was constructed based on field measurements and subsequently the C-10 cores were aligned to it. No adjustments to subbottom depths in C-10 sections were required to achieve a satisfactory match. The A-10/C-10 composite depth scale (referred to throughout as “depth”) is utilized for the production of geochemical proxy data and the age–depth model, in which sediment samples and radiocarbon-dated materials were derived primarily the A-10 cores and the C-10 cores were sampled to span gaps between core sections.

Table 1
AMS radiocarbon dates with calibrated 2 sigma error ranges. Samples highlighted with an asterisk (*) are omitted from the age model with explanations in the text.

Sample ID (UCIAMS#)	Core-drive	Drive depth (cm)	Total depth (cm)	Material	^{14}C age (^{14}C yr)	Error (yr)	Calib 6.0 age (yr BP)
89197	A-10 D1	45.0	45.0	Plant material	2535	30	2493–2745
109361	A-10 D1	66.5	66.5	Wood	3635	25	3872–4074
116878	A-10 D1	87.5	87.5	Plant material	4910	90	5470–5896
89198	A-10 D1	111.0	111.0	Plant material	6345	25	7174–7410
109362	A-10 D1	141.5	141.5	Wood	8850	110	9564–10,205
89199	A-10 D2	84.0	166.0	Plant material	9760	40	11,134–11,244
89200	A-10 D3	54.0	173.5	Seed	10,085	45	11,398–11,959
89122	C-10 D3	45.0	219.0	Wood	13,670	30	16,657–16,978
* 109363	A-10 D5	35.5	359.5	Plant material	14,590	550	16,570–18,903
89201	A-10 D7	29.0	553.0	Seed	25,300	510	29,173–31,074
* 89123	C-10 D7	64.0	598.0	Plant material	31,290	300	35,085–36,475
89124	C-10 D7	72.0	606.0	Wood	31,090	210	35,036–36,313
89121	A-10 D8	35.5	636.5	Wood	32,150	240	35,699–37,342

4.2. Chronology

The A-10/C-10 composite core age model, maximum variance between age control points, and linear sedimentation rates (cm/ka) are presented in Fig. 2. Two samples (UCIAMS # 109363 and # 89123) were excluded prior to generating the age–depth model. The first sample (UCIAMS # 109363) at 359.5 cm appears anomalously young compared with adjacent ages and, notably, had an extremely small CO_2 yield (0.017 mg C equivalent) prior to graphitization which approaches the threshold limit for AMS radiocarbon analysis. We suggest this sample was contaminated by modern carbon during the combustion and graphitization process given its extremely small mass (Oswald et al., 2005; Santos et al., 2010). In addition, inclusion of this date would require an abrupt increase in sedimentation rate that is not supported by any lithologic evidence or radiocarbon constraints. The second sample (UCIAMS # 89123) at 598 cm displays a modest age reversal with the adjacent sample (#89124) at 606 cm depth. The calibrated age distributions for both samples overlap and therefore we exclude the sample at 598 cm based on its lower carbon yield and slightly larger age uncertainty.

4.3. Lithostratigraphy

Our paleoenvironmental interpretation of the Burial Lake

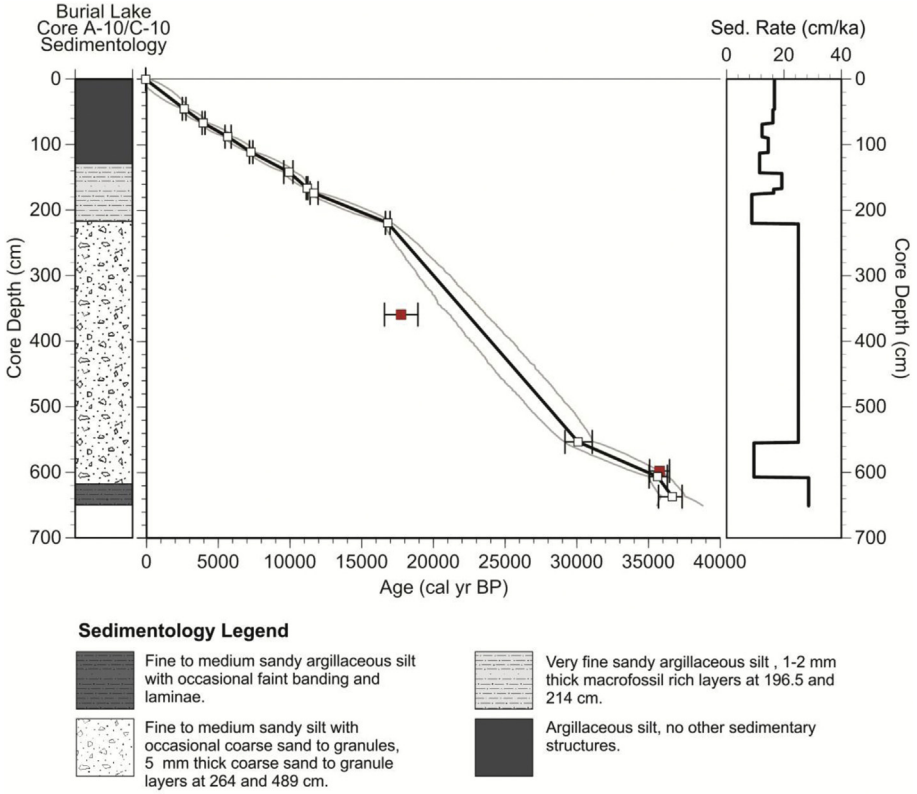

Fig. 2. Burial Lake A-10/C-10 composite core stratigraphic column showing sedimentology. Age–depth model developed from the AMS radiocarbon dates (black squares) with 2σ calibrated uncertainty generated with the CLAM code in R software (Blaauw, 2010) using point to point, linear interpolation (black line). Samples designated with a red square are rejected from the age model. The maximum variance between age control points is based on the 2σ calibrated ^{14}C ages calculated from 10,000 Monte Carlo simulations following a random draw from a normal distribution (Marcott et al., 2013). Sedimentation rates are calculated between contiguous ^{14}C dates and are presented in cm per thousand years (cm/ka). (For interpretation of the references to color in this figure legend, the reader is referred to the web version of this article.)

sediments is based on lithologic subunits from core descriptions (Fig. 2) and sediment physical and geochemical data (Figs. 3 and 4; Table 2; Supplemental Figs. 2 and 3). Variations in organic matter (wt %), biogenic silica (wt %), magnetic susceptibility, and the availability of macrofossils for radiocarbon analysis (Table 2; Fig. 5A, B) allow identification of 4 lithologic subunits. Comparison of C/N ratios with organic matter $\delta^{13}C$ (Fig. 5C) and organic matter $\delta^{13}C$ against $\delta^{15}N$ (Fig. 5D) indicates changes in the source (terrestrial versus aquatic) and isotopic composition of organic matter that is consistent with the identified subunits. Analysis of scanning XRF data indicates the Inc/Coh ratio is a sensitive indicator of sediment organic matter content (see Supplemental). Further, the matrix-corrected silicon ($Si_{(norm)}$) to titanium ratio ($Si_{(norm)}$/Ti) is a reliable proxy for sedimentary biogenic silica across subunits 3 and 4 spanning the last 16,500 cal yr BP (see Supplemental). Lithologic subunits broadly correspond to changes in sediment accumulation rates (Fig. 2), determined by calculating the time difference between contiguous 1 cm intervals across the composite A-10/C-10 core sequence.

4.4. Lithologic subunit 1 (651–540 cm depth)

Subunit 1 extends upward from the base of the composite core (651 cm) to 540 cm and spans the interval between 37,200 and 29,600 cal yr BP. The basal sediments from 651 to 618 cm consist of dark yellow brown (10YR 4/2) to grayish brown (5YR 3/2), fine to medium sandy argillaceous silt with occasional banding and faint laminae (Fig. 2). The upper portion from 618 to 540 cm consist of dark yellow brown (10YR 4/2) to grayish brown (5YR 3/2), fine to medium sandy argillaceous silt and a minor proportion of coarse sand and granules, with occasional banding and faint laminae (Fig. 2). The banding and faint laminae throughout subunit 1 presumably represent small variations in sediment organic matter content or subtle grain size variations. Powder XRD analysis of a sample at 613–614 cm indicate quartz is the dominant mineral phase present (Supplemental Fig. 6). Smear-slide analysis of several samples shows very few diatom frustules and a large proportion of silicate mineral matter. Subunit 1 sediments are characterized by relatively high and variable dry bulk density, magnetic susceptibility, and titanium values (Figs. 3 and 4; Table 2). Biogenic silica is low and stable, and indicates minimal aquatic productivity. Organic matter and Inc/Coh are low with little variability, and gradually decrease up-section towards the subunit 2 boundary. Organic matter $\delta^{13}C$ values are moderate to high and exhibit considerable variability, while organic matter $\delta^{15}N$ values gradually increase through subunit 1 (Fig. 3). C/N ratios are relatively low during this interval and gradually decrease up-section towards the Zone 2 boundary (Fig. 3).

4.5. Lithologic subunit 2 (540–217 cm depth)

Subunit 2 extends from 540 cm to 217 cm and spans the period between 29,600 and 16,500 cal yr BP. The contact with subunit 1 sediments is gradual and sediments primarily consist of dark yellow brown (10YR 4/2) to grayish brown (5YR 3/2), fine to medium sandy argillaceous silt and a minor proportion of coarse sand and granules (Fig. 2). Powder XRD analysis of samples at 449–450 cm, 321–32 cm, and 293–294 cm depth indicate quartz is the dominant mineral phase present (Supplemental Fig. 6). Smear-slide analysis of select samples from subunit 2 shows few diatom frustules and a large proportion of silicate mineral matter. Distinct layers of fine sand to granules are present from 489 to 489.5 cm and 264 to 264.5 cm. The layers compositionally represent a mix of lithologies, including mafic to felsic crystalline rocks, gray sandstone particles, and quartz grains that are sub-angular to sub-rounded in shape. The contact between the underlying and overlying finer sediments is horizontal and sharp. Although direct age control within subunit 2 is lacking, average sedimentation rates are the highest (at ~25 cm/ka). Plant macrofossils >63 μm are virtually absent in subunit 2 sediments, besides a small amount of grass isolated from sediment at 359–360 cm (UCIAMS # 109363). Subunit 2 is divided further into subunit 2a (540–289 cm) and subunit 2b (289–217 cm) based on subtle variability in the organic and inorganic geochemical proxies, many of which show a change in trend at the 2a/2b boundary.

4.6. Lithologic subunit 2a (540–289 cm depth)

Subunit 2a extends from 540 cm to 289 cm and spans the period between 29,600 and 19,600 cal yr BP. The sediments are characterized by high, variable, and gradually declining dry bulk density and the highest magnetic susceptibility and titanium values for the entire record (Figs. 3 and 4; Table 2). Biogenic silica values are uniformly low, stable, and similar to subunit 1 values. Organic matter is the lowest over the entire record and gradually decreases up-section in subunit 2a and attains the lowest values between 374

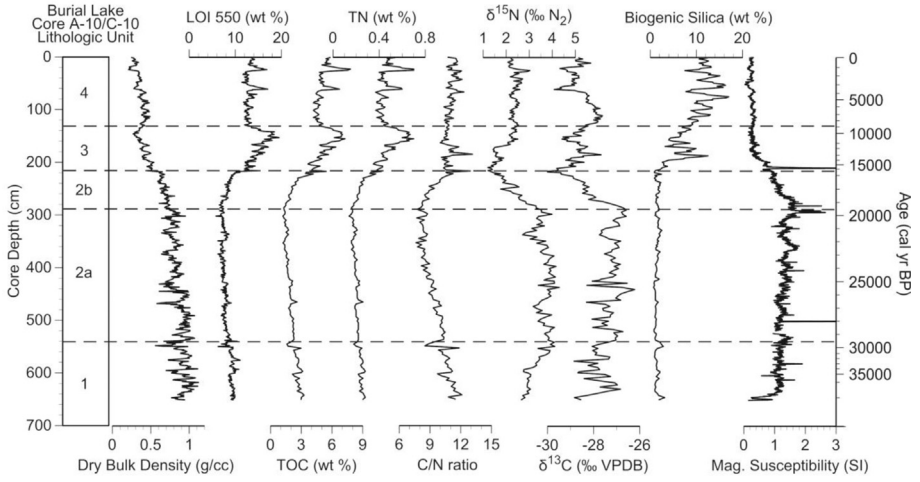

Fig. 3. Burial Lake A-10/C-10 composite core physical and organic proxy data plotted against depth (cm) and age (cal yr BP) with distinct lithologic subunits, identified primarily by variations in LOI 550 (wt %), biogenic silica (wt %), magnetic susceptibility, and the presence of plant macrofossils for radiocarbon dating.

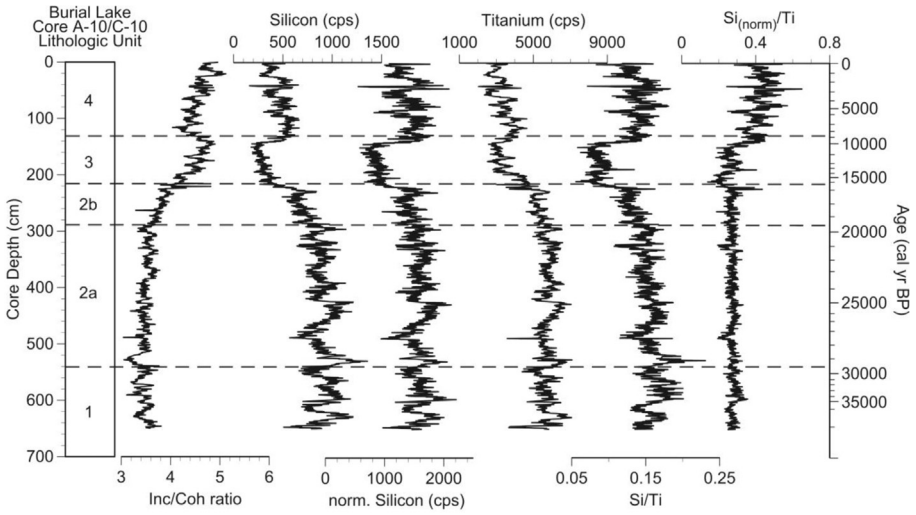

Fig. 4. Burial Lake A-10/C-10 composite core elemental abundances from scanning XRF analysis plotted against depth (cm) and age (cal yr BP) with distinct lithologic subunits.

Table 2
Burial Lake core A-10/C-10 lithologic subunits including depth (cm) intervals and age (cal yr BP) ranges. Mean values for the physical, geochemical, and elemental proxy data are reported for each respective lithologic subunit.

Lithologic subunit	Core depth cm	Age range cal yr BP	Dry BD g/cc	LOI 550 wt %	LOI 1000 wt %	Bio Si wt %	TOC wt %	TN wt %	C/N ratio
4	0–129	8800–2010 AD	0.36	13.1	0	11.6	5.05	0.45	11.1
3	129–217	16,500–8800	0.41	15.0	0	5.8	5.43	0.50	10.8
2b	217–289	19,600–16,500	0.68	7.6	0	1.6	2.29	0.24	9.3
2a	289–540	29,600–19,600	0.84	7.6	0	1.5	1.80	0.20	9.1
1	540–651	37,200–29,600	0.91	9.2	0	1.5	2.60	0.24	10.7

Lithologic subunit	Core depth cm	Age range cal yr BP	$\delta^{15}N$ ‰ N_2	$\delta^{13}C$ ‰ VPDB	Mag. Susc. 10^{-5} SI	Titanium cps	Inc/Coh	$Si_{(norm)}/Ti$
4	0–129	8800–2010 AD	2.37	−28.5	0.5	3300	4.5	0.42
3	129–217	16,500–8800	1.84	−28.8	0.5	3500	4.5	0.28
2b	217–289	19,600–16,500	2.35	−28.2	1.2	5200	3.8	0.28
2a	289–540	29,600–19,600	3.66	−27.2	1.3	5800	3.5	0.28
1	540–651	37,200–29,600	3.22	−27.8	1.1	5700	3.5	0.28

and 300 cm (Fig. 3). Inc/Coh values are low, stable, and similar to subunit 1 values. Organic matter $\delta^{13}C$ and $\delta^{15}N$ values are the highest (most positive) throughout the entire record and display considerable variability throughout subunit 2a (Fig. 3). C/N ratios gradually decrease from the base of subunit 2a up-section and attain the lowest values over the entire record toward the subunit 2b boundary (Fig. 3).

4.7. Lithologic subunit 2b (289–217 cm depth)

Subunit 2b extends from 289 cm to 217 cm and spans the period between 19,600 and 16,500 cal yr BP. The subunit 2b transition is marked by declining dry bulk density, magnetic susceptibility, and titanium values that continue towards the subunit 3 boundary (Figs. 3 and 4; Table 2). Biogenic silica values are low, stable, and similar to subunit 2a values. Organic matter, Inc/Coh, and C/N ratios gradually increase from their minimum values at the base of subunit 2b toward the subunit 3 boundary (Fig. 3). In addition, organic matter $\delta^{13}C$ and $\delta^{15}N$ gradually decrease from maximum values at the base of subunit 2b and attain their lowest (negative) values at the subunit 3 boundary (Fig. 3).

4.8. Lithologic subunit 3 (217–129 cm)

Subunit 3 extends from 217 cm to 129 cm and spans the period between 16,500 and 8800 cal yr BP. The contact with subunit 2b sediments is rather abrupt (in comparison to the subunit 1 and 2 transition) and sediments consist of homogenous dark yellow brown (10YR 4/2) to pale yellowish brown (10YR 6/2), very fine argillaceous sandy silt (Fig. 2). Powder XRD analysis of a sample at 129–130 cm indicates quartz is the dominant mineral phase present (Supplemental Fig. 6). Organic macrofossil rich, 1–2 mm thick layers are present at 196.5 and 214 cm, respectively. Smear-slide analysis of select samples from subunit 3 shows a substantial increase in the proportion of diatom frustules with no evidence of dissolution and abundant silicate mineral matter. The subunit 3 transition is characterized by declining and lower dry bulk density, titanium, magnetic susceptibility (Figs. 3 and 4; Table 2), and a lower but variable sedimentation rate (9–19 cm/ka), in comparison with the previous (subunit 2) interval. An abrupt spike in magnetic susceptibility occurs at ~210 cm (Fig. 3) and represents a brief return to higher values. Biogenic silica values increase up-section from the base of subunit 3, subsequently peak at 12.5% at 186 cm, and fluctuate and gradually decrease up-section toward the subunit 4 transition (Fig. 3). $Si_{(norm)}/Ti$ values track the general trends in biogenic silica through subunit 3 (Fig. 4). Organic matter and Inc/Coh values increase up-section from the base of subunit 3 and peak at the highest values over the entire record between 153 and 141 cm (10,500–9900 cal yr BP). Organic matter $\delta^{13}C$ values are lower on average compared with subunit 1 and 2 sediments, and

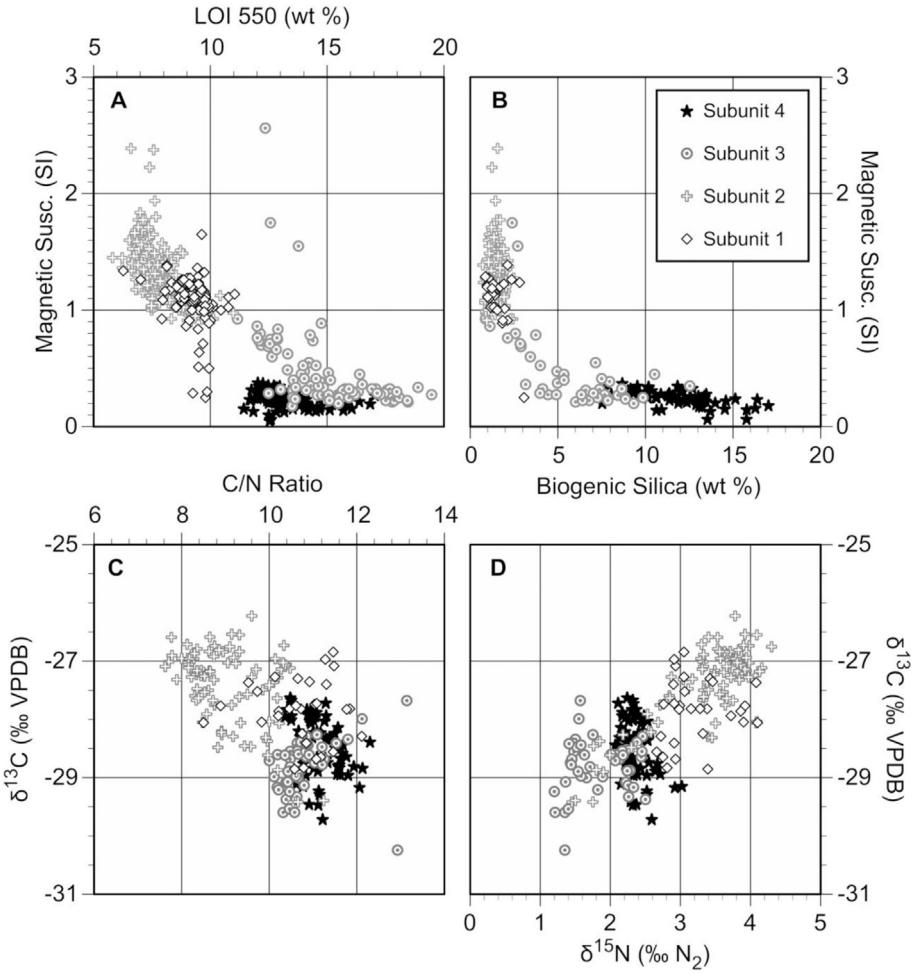

Fig. 5. Scatterplots of Burial Lake A-10/C-10 composite core proxy data by lithologic subunit showing distinct clustering, including A) magnetic susceptibility (SI) against LOI 550 (wt %), B) magnetic susceptibility (SI) against Biogenic Silica (wt %), C) organic matter $\delta^{13}C$ (‰ VPDB) against C/N ratio, and D) organic matter $\delta^{13}C$ (‰ VPDB) against organic matter $\delta^{15}N$ (‰ N_2).

fluctuate substantially throughout subunit 3 (Fig. 3; Table 2). Similarly, organic matter $\delta^{15}N$ values are lower but generally more stable compared with the previous lithologic zones. C/N ratios are on average the highest throughout subunit 3 (Fig. 3), and the record is punctuated by several abrupt increases. A greater abundance of plant macrofossils for radiocarbon dating is evident in subunit 3 and sedimentations rates are relatively low (13 cm/ka average).

4.9. Lithologic subunit 4 (129–0 cm)

Subunit 4 extends from 129 cm to the core top and spans the interval between 8800 cal yr BP and A.D. 2010. The contact with subunit 3 is gradual and sediments consist of homogenous grayish brown (5YR 3/2) to dusky brown (5YR 2/2), argillaceous silt sediment with no obvious sedimentary structures (Fig. 2). Smear-slide analysis of select samples from subunit 4 shows a general abundance and diversity of diatom frustules, no obvious evidence of dissolution, and substantial variability in diatom proportion over intervals of 5–10 cm. Further, smear-slides show an abundance of silicate mineral matter. Subunit 4 sediments are characterized by low dry bulk density, titanium, and magnetic susceptibility values (Figs. 3 and 4; Table 2). Organic matter content is generally stable and intermediate, compared to higher values in subunit 3 and lower values in subunits 1 and 2. In contrast, Inc/Coh values gradually increase throughout subunit 4 and attain the highest values over the entire record over the upper 15 cm. Organic matter $\delta^{13}C$ values are higher on average than subunit 3 with a range of ~1‰, while $\delta^{15}N$ values are generally stable and more positive compared to subunit 3 sediments. C/N ratios increase slightly up-core and are higher on average than any time previously. Biogenic silica and $Si_{(norm)}$/Ti values are higher than any time during the entire record and display substantial variability over 5–10 cm intervals (Figs. 3 and 4). Plant macrofossils are present throughout subunit 4 sediments and sedimentation rates are low (15 cm/ka average) and generally stable.

5. Discussion

The Burial Lake sediment record from the basin depocenter shows no evidence of major unconformities (e.g. mud cracks, erosional surfaces, etc.) found in intermediate water depth cores (Abbott et al., 2010) that would indicate discontinuous sedimentation in the deepest part of the basin. However, the distinct 5 mm thick sand and granule layers at 264 cm and 489 cm provide sedimentological evidence for a high energy transport process at the lake depocenter. Given the lack of a surficial inlet, we hypothesize the sediments are reworked from the shoreline during a period of lower lake level (Abbott et al., 2010), when the lake surface area was much smaller and the distance from shoreline to depocenter was substantially reduced. The coarse sediment layers

seem unlikely to represent turbidity flows and re-working of shelf sediments as they have sharp upper and lower contacts and a lack of textural grading. The coarse layers could represent sub-aerially exposed shoreline sediments or a lag from winnowing of fine sediments in a very shallow lake from wave-base erosion, both of which might result in disconformities. Unfortunately, radiocarbon constraints throughout lithologic subunit 2 are lacking to directly assess the possibility of these layers representing disconformities. We suggest the nature of the coarse sediment layer contacts (i.e. horizontal and sharp), minimal thickness (only 5 mm), and no obvious evidence for an unconformity indicate the features do not represent discontinuous sedimentation. In contrast, the major unconformity present in the intermediate water depth cores from Burial Lake is characterized by a clear erosional and irregular contact (Abbott et al., 2010). The underlying ~30 cm of sediment consists of sand and gravel, interpreted to reflect a lag-deposit formed via deflation and winnowing of fine sediments, which is sedimentologically distinct compared with the coarse layers in the depocenter cores. We therefore suggest the Burial Lake sediment record is continuous and spans the last 37,200 cal yr BP. However, we acknowledge that age control between 219 cm and 553 cm spanning the period between 16,800 and 30,100 cal yr BP (median ages) is based on a linear interpolation (Fig. 2), and therefore the timing of paleoenvironmental transitions cannot be accurately determined during this period.

We integrate our results with a complimentary environmental magnetic investigation from Burial Lake (Dorfman et al., in this issue) and focus our comparison on S-ratios (Fig. 6), a sensitive indicator of dust input to the lake. Higher S-ratios are interpreted to reflect periods of increased dust accumulation while lower values indicate periods of diminished flux. In addition, we present a relative lake-level curve (Fig. 6) based on previous work of Burial Lake sediments (Abbott et al., 2010) and integrate the results from a chironomid-inferred temperature reconstruction (Kurek et al., 2009). To ensure consistency, the radiocarbon and age model data are updated using the IntCAL09 calibration curve (Reimer et al., 2009) and slight adjustments are made based on proxy data reported in this study (see Supplemental).

5.1. Interpretation of the carbon and nitrogen isotopic composition of organic matter

The carbon stable isotopic composition ($\delta^{13}C$) of organic matter in lake sediments is controlled by several factors including the contribution of various sources (algal, terrestrial) and changes in the respective photosynthetic pathways, changes in aquatic productivity, and the $\delta^{13}C$ of dissolved inorganic carbon (DIC) inputs to a lake (Meyers and Ishiwatari, 1993; Meyers and Teranes, 2001; Finney et al., 2012). Variations in Burial Lake C/N ratios, which assess the relative proportion of terrestrial (C/N > 20) versus aquatic (C/N < 10) source inputs (Meyers and Teranes, 2001), indicate a mixed algal–terrestrial and at times primarily algal source of organic matter over the last 37,000 years (Fig. 6). In addition, when the organic matter source is predominantly aquatic, we hypothesize that variations in $\delta^{13}C$ are also controlled by changes in aquatic productivity and the $\delta^{13}C$ of CO_2 supplied to Burial Lake for algal utilization. Increasing algal productivity levels correspond with higher $\delta^{13}C$ values, and vice versa for decreasing productivity (Meyers and Teranes, 2001). Further, changes in the $\delta^{13}C$ of dissolved CO_2 supplied to Alaskan lakes have been shown to influence the $\delta^{13}C$ of sedimentary organic matter (Finney et al., 2012). Many Alaskan lakes have surface water pCO_2 concentrations above atmospheric levels, due to inputs of watershed-respired CO_2 from permafrost or organic rich soils (Kling et al., 1991). In such lacustrine systems, increased inputs of watershed-respired CO_2 with relatively low $\delta^{13}C$ values typical of C_3 plants (~−27‰) results in relatively low $\delta^{13}C$ organic matter content (Finney et al., 2012). The pCO_2 of two surface water samples from Burial Lake were supersaturated (481 ppm, 509 ppm) with respect to equilibrium with the atmosphere, providing evidence that inputs of watershed respiration products affect the $\delta^{13}C$ of dissolved inorganic carbon inputs to the lake. Therefore, we interpret organic matter $\delta^{13}C$ trends in light of source changes, with further variation related to changes in productivity and from variable inputs of landscape derived and respired organic matter.

The interpretation of the nitrogen stable isotopic composition ($\delta^{15}N$) of organic matter is hindered by our lack of modern watershed and limnological data on nitrogen cycling at Burial Lake. Variations in the $\delta^{15}N$ of organic matter might reflect changing productivity and the relative sources and isotopic composition of nitrogen supplied to lakes (Hu et al., 2001; Meyers and Teranes, 2001). In addition, the $\delta^{15}N$ of sedimentary organic matter might be controlled by variations in the availability of reactive nitrogen (relative supply versus demand) inputs arising from hydroclimate variability. Global-scale studies have found that soil and plant $\delta^{15}N$ values increase with decreasing precipitation and increasing N availability (Amundson et al., 2003; Craine et al., 2009), indicating that climate plays a significant role in N cycling. Thus, we interpret organic matter $\delta^{15}N$ trends in the Burial Lake sediment record to reflect a combination of changes in productivity and the availability of reactive nitrogen driven by hydroclimate.

5.2. The mid-Wisconsin interstadial (37,200–29,600 cal yr BP)

The presence of fine to medium sandy argillaceous silt with relatively intermediate organic content at the base of lithologic subunit 1 (Fig. 2), in conjunction with core-transect data, suggest lake levels remained at intermediate to high levels between 37,200 and 36,100 cal yr BP. Specifically, core-transect data indicate lake levels were >12.4 m below overflow level (BOL) between 37,200 and 33,000 cal yr BP (Fig. 6). An erosional unconformity in intermediate water depth core C-98 from Burial Lake indicates a drop in lake level below 11.3 m water depth occurred sometime after 33,000 cal yr BP (Abbott et al., 2010). The transition to coarser sediments (fine to medium sandy argillaceous silt with coarse sand and granules) at 36,100 cal yr BP that persists until 16,500 cal yr BP indicates a change in paleoenvironmental conditions relative to the preceding period at Burial Lake. The lithology during this period is consistent with the process of ice-rafting over the lake (e.g. Smith, 2000). Alternatively, the granules could originate from aeolian transport and deposition on the frozen lake surface, with subsequent melting resulting in drop stone deposition (e.g. Lewis et al., 2002). Today, lake ice covers the modern system for 9 months a year, yet coarse sediments (coarse sand to granules) are absent for the last 16,500 cal yr BP. Accordingly, we favor an increase in aeolian activity to explain the coarser sediments. This assertion is supported by relatively high magnetic susceptibility and titanium concentrations over subunit 1, and the distinct magnetic signature originating from wind-blown (aeolian) sources (Dorfman et al., in this issue). Potential local sources of aeolian input to the lake at this time include alluvial sediments along aggrading rivers and sub-aerially exposed glaciolacustrine sediments (Hamilton, 2001), while a far afield source could originate from the exposed Chukchi continental shelf (Dorfman et al., in this issue). Low and gradually declining C/N ratios and relatively heavy (positive) organic matter $\delta^{13}C$ values indicate organic matter originated primarily from aquatic (in-lake) sources (Meyers and Ishiwatari, 1993; Finney et al., 2012), though the low organic matter and biogenic silica values attest to low levels of aquatic productivity (Fig. 6). The gradual increase in $\delta^{15}N$ values through the mid-Wisconsin interstadial

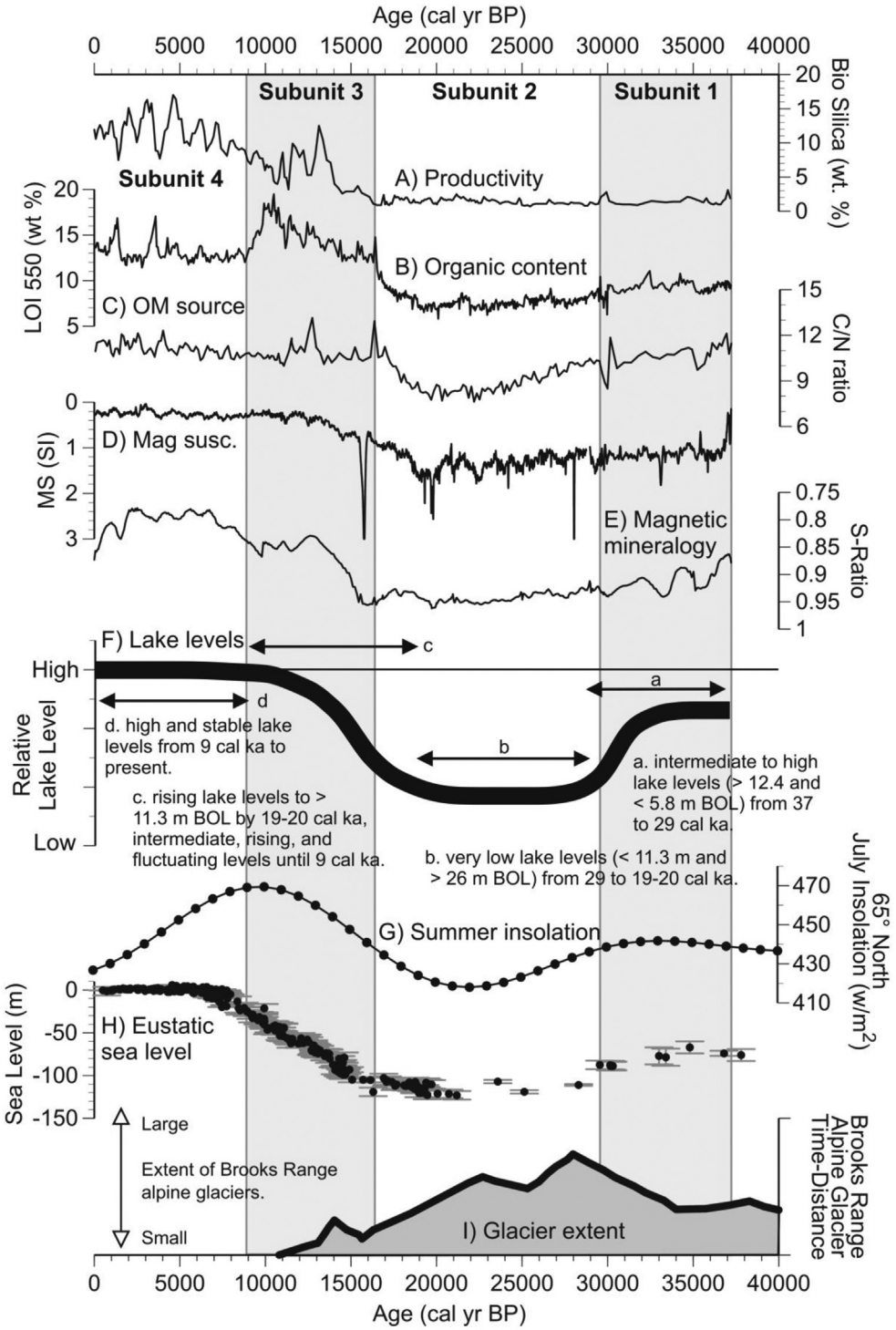

Fig. 6. Burial Lake A-10/C-10 composite core proxy data including A) biogenic silica, B) LOI 550, C) C/N ratio, D) magnetic susceptibility (SI), E) S-ratio that describes the relative proportion of low coercivity to high coercivity magnetic material, which is interpreted to reflect the regional input of dust into to Burial Lake (Dorfman et al., in this issue), and F) Burial Lake estimated lake level curve in meters (m) below overflow level (BOL) (Abbott et al., 2010). The data is also compared to G) 65° North July insolation (Berger and Loutre, 1991), H) relative eustatic sea level (Clark et al., 2009 and references therein), and I) time–distance diagram of Brooks Range, Alaska alpine glacier extent (Briner and Kaufman, 2008).

(Fig. 3) corresponds with increasing aridity and lower lake-levels (Fig. 6), suggesting that changes in $\delta^{15}N$ reflect changing hydroclimate conditions and relatively high N availability (compared with demand) (Amundson et al., 2003; Craine et al., 2009). Palynological evidence from the C-98 core indicates a tundra landscape with cool and dry conditions compared with the present (Abbott et al., 2010). Overall, proxy evidence from this study and core-transect data demonstrate relatively high lake levels and an interstadial climate with slightly drier and windy conditions compared to the present.

Evidence from Burial Lake provides additional support for interstadial climate conditions >30,000 cal yr BP in eastern Beringia

with warmer and slightly wetter conditions compared with the LGM (Anderson and Lozhkin, 2001 and references therein). In the Noatak Basin, interstadial conditions are reported between 36 and 30 ka ^{14}C years from organic floodplain deposits and palaeosols along Noatak River (Hamilton, 2001). Additional lake records have since been reported from Zagoskin Lake (Fig. 1) and Arolik Lake in western Alaska, respectively that show slightly more mesic conditions than the following full glacial interval (Ager, 2003; Kaufman et al., 2003). Interstadial conditions occur during a time of relatively high Northern Hemisphere summer insolation, reduced alpine glacier extent, and when eustatic sea levels were −80 to −60 m lower than modern conditions (Fig. 6). These intermediate sea levels would have reduced the extent of subaerial Bering Sea continental shelf exposure compared with the LGM lowstand. As a result, the transport distance of moisture-laden air masses from the North Pacific Ocean traveling towards Alaska would have been similar to that during the Lateglacial transition (14,000–16,000 cal yr BP) where notable increases in effective moisture and higher lake-levels are reported across interior and northern Alaska (Abbott et al., 2000; Mann et al., 2002; Finkenbinder et al., 2014; Gaglioti et al., 2014).

5.3. The Last Glacial Maximum (29,600–19,600 cal yr BP)

Burial Lake sediments and proxy data across lithologic subunit 2 indicate a two-phase structure that corresponds to the LGM (29,600–19,600 cal yr BP) and the last deglaciation (19,600–16,500 cal yr BP). The highest magnetic susceptibility values and relatively high titanium concentrations between 29,600 and 19,600 cal yr BP suggests a substantial flux of mineral sediments, which likely originated from wind-blown sources (Dorfman et al., in this issue). The lowest C/N ratios indicate organic matter was primarily sourced from aquatic (in-lake) sources (Meyers and Ishiwatari, 1993) during the LGM.

The relatively high δ^{13}C values coincide with the period of lowest lake-levels and the deposition of coarse-grained minerogenic sediments. We interpret organic matter δ^{13}C trends to reflect changes driven by decreased productivity and possibly decreased inputs of landscape derived and respired organic matter during this period of dry and cold conditions. Further, δ^{15}N values are the highest at any time during the record and coincide with the period of low lake levels, again suggesting that aridity controls δ^{15}N through the LGM. Sustained low levels of organic matter and biogenic silica during the LGM indicate aquatic productivity was minimal likely due to cold conditions and a short ice free, growing season.

The Burial Lake proxy data support existing evidence for extremely arid and windy conditions during the LGM in Arctic Alaska. Evidence for low lake levels and arid conditions at Burial Lake are supported internally by the presence of an erosional unconformity in the C-98 core with a gap in sedimentation between 33,000 and 24,300 cal yr BP. Abbott et al. (2010) suggest that sedimentation resumed at the C-98 core site by 24,300 cal yr BP, and therefore interpret the early LGM to be the driest period over the entire record. However, this age assignment is extrapolated from a radiocarbon date of 19,880 cal yr BP that is 51 cm above an erosional unconformity (see Supplemental). Alternatively, the transition to higher lake-levels is constrained directly to before 19,880 cal yr BP. Our continuous proxy data showing coarse sediments (Fig. 2) and relatively low organic content (Fig. 6) are consistent with persistently dry conditions throughout the LGM. Several other lake sediment records from northwest Alaska show evidence for lower lake levels during the LGM (Anderson, 1988; Oswald et al., 1999; Mann et al., 2002) when most small, shallow lakes in the interior of Alaska were dry (Abbott et al., 2000). Thus, evidence from Burial Lake provides additional support for the west–east moisture gradient in Alaska during the LGM, which has been attributed to proximity to marine moisture sources (Guthrie, 2001). The period of low lake levels and minimal aquatic productivity corresponds to the time when most ice sheets attained their maximum late-Wisconsin extent (Clark et al., 2009 and references therein) and the LGM sea level lowstand (Fig. 6). As a result, the Bering Land Bridge attained its greatest extent as lower sea levels exposed the shallow Bering and Chukchi continental shelves (Hopkins, 1982), thereby enhancing the continentality of interior regions in Alaska.

Alpine glaciers in the central Brooks Range attained their maximum extent during the early LGM between 27,000 and 25,500 cal yr BP and experienced a later retreat and re-advance to near the LGM maxima position after 23,000 cal yr BP (Fig. 6) (Hamilton, 1982; Briner and Kaufman, 2008). The relatively early LGM maximum extent of alpine glaciers in the Brooks Range, compared with elsewhere in Alaska (Briner and Kaufman, 2008), suggests a complex pattern in glacier mass balance. Our reinterpretation of lake-levels at Burial Lake across the LGM (Fig. 6; see Supplemental) and proxy data from this study indicates sustained low lake levels and very low effective moisture levels between 29,600 and ~20,000 cal yr BP. Although our age control is limited through the LGM, we suggest the relatively early LGM in the central Brooks Range could have occurred during a time of slightly higher effective moisture levels. Therefore, we hypothesize that subsequent more extensive advances were possibly precluded by greater aridity as the Bering Land Bridge increased in size and the distance from marine moisture sources increased.

5.4. The last deglaciation (19,600–16,500 cal yr BP)

Numerous proxies in the Burial Lake record change in trend around ~19,600 cal yr BP at the subunit 2b transition (Figs. 3 and 4) consistent with considerable environmental change initiating at this time. Specifically, organic matter concentrations and C/N ratios gradually increase up-section while magnetic susceptibility, titanium, and organic matter δ^{13}C and δ^{15}N values gradually decrease up-section towards the subunit 3 boundary (Figs. 3 and 4). We interpret these changes to reflect a progressive increase in terrestrial organic matter flux and a corresponding decrease in clastic sediment delivery to the lake. The decrease in organic matter δ^{15}N values could reflect this increase in terrestrial organic matter because land plants are generally lower in δ^{15}N (Meyers and Teranes, 2001). Decreasing δ^{15}N values corresponds with rising and higher lake levels at Burial Lake, consistent with increasing supply of reactive N (compared with demand) and the aforementioned relationship between δ^{15}N and hydroclimate (Amundson et al., 2003). The trend to decreasing organic matter δ^{13}C values, coincident with increasing C/N values, likely reflects increased inputs of watershed-respired CO_2 from the catchment (Finney et al., 2012).

We acknowledge the lack of direct age control limits a precise age determination for this transition (Fig. 2). Assuming a constant sediment accumulation rate at Burial Lake through LGM, the estimated uncertainty in the timing of this transition is between 20,700 and 18,600 cal yr BP. However, given the considerable climatic change that transpired in the Alaskan Arctic through the LGM (Hamilton, 2001; Kurek et al., 2009; Abbott et al., 2010), it is very likely that sedimentation rates at Burial Lake were variable and the error estimates associated with this transition could be even greater. Nonetheless, support for major environmental change occurring around this time is provided by the C-98 core, which shows rising and higher lake levels by 19,880 cal yr BP (Fig. 6). Increasingly mesic conditions beginning at 19,800 cal yr BP inferred

from palynological data (Abbott et al., 2010) also coincide with the last deglaciation sediment transition.

The last deglaciation transition is broadly synchronous with gradually rising high-latitude Northern Hemisphere summer insolation (Berger and Loutre, 1991) and retreat of alpine glaciers in the Central Brooks Range between 22,000 and 18,500 cal yr BP (Hamilton, 1982) (Fig. 6). Further evidence for climatic change during this period is provided by a chironomid-inferred July temperature reconstruction from Burial Lake, which shows sustained cold temperatures through the LGM until ~17,400 cal yr BP (Kurek et al., 2009). Reconstructed July temperatures gradually increase after ~17,400 cal yr BP and reflect increasingly warmer and longer summers. Increasing temperatures are broadly synchronous with rising global atmospheric CO_2 levels beginning around ~17,000 cal yr BP (Monnin et al., 2001). We therefore suggest the changing trend in sediment properties at ~19,600 cal yr BP along with corresponding increases in *Cyperaceae* and *Salix* (Abbott et al., 2010) are driven by increasing effective moisture levels coincident with rising and higher lake-levels (Fig. 6). Increasing effective moisture levels at this time are possibly related to initial retreat of the Laurentide Ice Sheet at ~19,000 cal yr BP (Dyke, 2004) and a reorganization in atmospheric circulation across eastern Beringia. Interestingly, a chironomid-inferred July temperature reconstruction from Zagoskin Lake in western Alaska shows progressive warming of ~3 °C between 25,000 and 17,000 cal yr BP (Kurek et al., 2009), possibly reflecting spatial variations in climatic conditions in western Alaska at this time.

5.5. The Lateglacial and early Holocene thermal maximum (16,500–8800 cal yr BP)

The Lateglacial transition at Burial Lake beginning at ~16,500 cal yr BP is marked by an abrupt change in sedimentology, with decreasing grain size (very fine sandy argillaceous silt) and absence of coarse sediments (granules) that characterized mid-Wisconsin interstadial, LGM, and the last deglaciation age sediments. Plant macrofossil abundance increases, suggesting more established vegetation in the surrounding catchment, and sedimentation rates are slower (9–19 cm/ka). Magnetic susceptibility and titanium values continue to gradually decrease through the Lateglacial, which we interpret a result of decreased windiness, stabilization of watershed soils, and from rising and higher lake-levels (Fig. 6). Rising and variable biogenic silica and $Si/Ti_{(norm)}$, and a corresponding increase in the presence and diversity in diatom frustules, indicates increased in-lake (aquatic) productivity likely due to a longer ice-free growing season and increasing nutrient flux to the lake. Relatively high and variable C/N ratios indicate a higher proportion of organic matter from terrestrial sources during this time, despite the increasing productivity. Organic matter $\delta^{15}N$ values attain their most negative values between 16,500 and 11,350 cal yr BP at the same time both terrestrial and aquatic productivity levels are increasing or higher than any previous time. Therefore, we interpret $\delta^{15}N$ changes in both decreased relative nitrogen availability relative to demand and increasing input of terrestrial organic matter to the sediment, both of which tend to decrease organic $\delta^{15}N$ (Meyers and Teranes, 2001; Craine et al., 2009). Overall, proxy evidence indicates the Lateglacial and Early Holocene between 16,500 and 8800 cal yr BP was a time of considerable climatic change with increasing and higher levels of terrestrial and aquatic productivity, decreased windiness and landscape stabilization, and continued rising lake-levels (Fig. 6) and increasing effective moisture.

The Lateglacial transition at Burial Lake beginning at 16,500 cal yr BP coincides with a decrease in dust accumulation inferred from decreasing and lower S-ratios (Fig. 6) (Dorfman et al., in this issue). Changing oceanographic conditions in the Bering Sea also indicate broadly synchronous ocean–land responses to warmer climate conditions around this time. For example, Caissie et al. (2010) report a transition from thick perennial pack ice to extensive sea ice with short periods of open water at Umnak Plateaus in the southern Bering Sea beginning at 16,900 cal yr BP. The deglacial transition at 16,500 cal yr BP coincides with evidence of alpine glacier retreat from the range front in the central Brooks Range before ~16,000 and 15,000 cal yr BP, and further retreat into cirques by ~14,000 cal yr BP (Badding et al., 2013). However, Hamilton (2003b) reports evidence of a minor re-advance of alpine glaciers in the central Brooks Range between 15,100 and 13,000 cal yr BP, possibly related to increased effective moisture levels, although geomorphic evidence (moraines) for this advance are lacking. Further, rising eustatic sea levels (Fig. 6) gradually flooded the Bering Land Bridge and reduced the transport distance of air masses to the Alaskan interior, effectively reducing the continentality of the Alaskan interior. Complete submergence of the Bering Land Bridge occurred between 12,000 and 11,000 cal yr BP (Elias et al., 1996; Keigwin et al., 2006), establishing the approximately modern continental configuration of Alaska.

The proxy evidence from Burial Lake is also consistent with other lacustrine records from Alaska that shows considerable and rapid environmental change initiated during the Lateglacial period. For example, Mann et al. (2002) report evidence of higher and fluctuating lake-levels, compared with the preceding glacial period, from Lake of the Pleistocene (Nikivlik Lake) (Fig. 1). Relatively high lake-levels and increased effective moisture levels occur between 12,500 and 11,000 ^{14}C yr BP and after 10,000 ^{14}C yr BP, while falling and lower lake-levels with decreased effective moisture occur between 11,000 and 10,000 ^{14}C yr BP (Mann et al., 2002). In addition, core-transect based lake-level reconstructions from Birch Lake (Abbott et al., 2000) and Harding Lake (Finkenbinder et al., 2014) in the interior of Alaska (Fig. 1) show relatively higher but variable lake-levels with increased effective moisture between 15,000 and 9000 cal yr BP, compared with LGM conditions. Pollen evidence from Burial Lake show a trend to more mesic conditions between 19,800 and 13,900 cal yr BP. Further, an abrupt rise in *Betula* pollen at Burial Lake at 13,900 cal yr BP (Abbott et al., 2010), combined with regional evidence for increasing shrub abundance during the Lateglacial (Anderson and Brubaker, 1994; Oswald et al., 1999; Higuera et al., 2009), provide additional evidence for warmer and wetter conditions at this time. The July temperature reconstruction from Burial Lake shows gradually rising temperatures beginning at ~17,000 cal yr BP that continued to rise to the highest levels over the entire record at 12,300 cal yr BP (Kurek et al., 2009).

Relatively low biogenic silica content and reduced aquatic productivity at Burial Lake between 13,000 and 12,400 cal yr BP possibly provides evidence for climatic deterioration during the early Younger Dryas (YD) in Alaska. However, the midge-inferred summer temperatures increase and peak at Burial Lake through the early YD (Kurek et al., 2009). Further, the apparent lack of a clear YD signal in other physical, geochemical, or elemental proxies (Figs. 3 and 4) suggests the absence of a strong climatic reversal at this time. This conclusion is consistent with the lack of evidence for YD alpine glacier advances in the central Brooks Range (Hamilton, 1982; Badding et al., 2013) and a review of paleoecological data showing similar to modern temperatures in northern Alaska (Kokorowski et al., 2008). However, this contrasts with regional evidence for the YD in northern Alaska that include low lake-levels and decreased effective moisture at Lake of the Pleistocene (Mann et al., 2002; Gaglioti et al., 2014) and floodplain incision on the Alaskan North Slope (Mann et al., 2010) from cooler and potentially drier conditions. Further, evidence for colder temperatures is inferred from fossil beetle assemblages along Noatak River (Elias,

2000) and from a negative $\delta^{18}O$ excursion from the Barrow ice wedge system on the Alaskan North Slope (Fig. 1) (Meyer et al., 2010). The apparently discordant evidence for the YD in northern Alaska could reflect seasonal differences in the sensitivity of proxies to environmental or climatic changes used in this study.

The peak in organic content over the entire record along with moderate C/N ratios at Burial Lake occurs between 10,500 and 9900 cal yr BP. We interpret this to reflect relatively high terrestrial productivity, which coincides with the latter part of the HTM in Alaska (Kaufman et al., 2004) and with the peak in sea surface temperatures in the northwest Pacific Ocean and Bering Sea (Max et al., 2012) over the last 15,000 years. Regionally, high productivity also coincides with the peak in thermokarst lake development across the circum Arctic (Walter et al., 2007) and peatland initiation across Alaska (Jones and Yu, 2010). Holocene to late Pleistocene age solifluction deposits mapped immediately north of Burial Lake (Hamilton, 2010) represent a local source of autochthonous organic matter delivered to the lake from permafrost degradation at this time. Additional evidence for regional summertime warming and increased effective moisture between 11,500 and 9500 cal yr BP is evinced from a period of floodplain aggradation and expansion of *Populus balsamifera* trees in the Arctic foothills (Mann et al., 2010). These coincident land–ocean environmental changes apparently reflect broadly synchronous responses to the summer insolation maxima (Berger and Loutre, 1991) during the early Holocene in the western Arctic.

5.6. The early Holocene to the present (A.D. 2010)

Burial Lake sediments spanning the early Holocene (8800 cal yr BP) to the present (A.D. 2010) consist of fine (argillaceous silt) sediment and combined with core-transect data, indicate high and generally stable lake-levels (Fig. 6). Low and relatively stable magnetic susceptibility and titanium content are consistent with a low clastic sediments flux, with minimal aeolian sedimentation (Dorfman et al., in this issue). Generally stable organic matter content and moderate C/N ratios indicate that organic matter primarily originated from a mixed aquatic-terrestrial source through this interval. Organic matter $\delta^{15}N$ values display only minor variability throughout the middle to late Holocene, suggesting that organic N-cycling and the source of reactive N for aquatic productivity remained relatively constant. Excursions to relatively negative $\delta^{13}C$ values also occur at 3580 and 1170 cal yr BP and likely reflect a variable flux of terrestrial organic matter delivered to the lake from the catchment. Pollen evidence from Burial Lake shows the *Alnus crispa* expansion occurred at 9000 cal yr BP and the vegetational mosaic thereafter is moist shrub tundra (Abbott et al., 2010).

The proxy data from Burial Lake spanning the early to late Holocene are consistent with regional-wide evidence for high and generally stable lake levels (Abbott et al., 2000; Finkenbinder et al., 2014), soil development and stabilization (Hu et al., 2001), and increasing and higher levels of aquatic and terrestrial productivity (Hu et al., 2001, 2003; Kaufman et al., 2003; Finney et al., 2012; Finkenbinder et al., 2014). For instance, biogenic silica displays large fluctuations and varies from ~6 to ~18 (wt. %) at multi-century to millennial time scales over the last 8800 cal yr BP (Fig. 6). We interpret changes in biogenic silica to reflect changes in aquatic productivity, given the generally linear sediment accumulation rate over the Holocene (Fig. 2), no evidence for diatom dissolution, and minimal variability in LOI 550 and TOC (Fig. 3). Unfortunately, the existing age model and temporal resolution of our biogenic silica record (average 140 yr/sample) do not allow us to address if these changes are related to Holocene millennial variability observed in other paleo records (Bond et al., 2001; Hu et al., 2003; Darby et al., 2012) or to assess the precise mechanism that drives aquatic productivity at Burial Lake. Relatively low S-ratios indicate diminished dust accumulation at Burial Lake compared with the preceding early Holocene and Lateglacial (Fig. 6). However, increasing S-ratios after ~2000 cal yr BP possibly reflect increasing dust accumulation at Burial Lake, which Dorfman et al. (in this issue) suggest could result from late Holocene alpine glacier advances in the Brooks Range.

6. Summary

The Burial Lake record provides one of the oldest lacustrine records from the North American Arctic to continuously span the period prior to the last glacial period through to the present. Our multi-proxy analysis provides new insights into the sensitivity of Arctic ecosystems to climatic, environmental, and landscape changes across glacial to interglacial timescales. Unfortunately, the absence of macrofossils for radiocarbon dating across the LGM and last deglaciation, during the period of cold, extremely arid, and windy conditions, limits our ability to accurately determine the precise timing of environmental changes at key times. Further, the lack of evidence for dramatic environmental changes throughout the LGM and across the Younger Dryas, could suggest the physical and geochemical proxies used in this study were possibly less sensitive to climatic changes at these times. Alternately, the absence of evidence for environmental changes could reflect seasonal differences in the sensitivity of productivity proxies (organic content, biogenic silica) used in this study, which primarily respond to summer growing season conditions. These apparent discrepancies highlight the need to carefully interpret proxy indicators to infer environmental changes, which by their nature respond to myriad environmental factors and often towards seasonal climate conditions.

Acknowledgments

Funding for this project was provided by the National Science Foundation (NSF-ARC 0909545) to Abbott and Stoner. Finkenbinder recognizes support from the University of Pittsburgh Mellon Predoctoral Fellowship during the writing of this manuscript. We would like to thank Dr. Nathan Stansell for his help with fieldwork at Burial Lake in the summer of 2010; John Southon, Guaciarra dos Santos and prep-lab personnel (Chanda Bertrand, Hector Martinez, and Shari Bush) at the Keck Carbon Cycle Accelerator Mass Spectrometry Laboratory at the University of California, Irvine for assistance in preparing graphite targets and radiocarbon measurement; Dr. Emily Elliot for her assistance and use of the UV-VIS spectrophotometer for biogenic silica measurement; Aubrey Hillman and David Pompeani for helpful ideas and discussion with the research; and Darren Larsen for review of an early version of the manuscript. We also thank the editor and comments from two anonymous reviewers that greatly improved the manuscript.

Appendix A. Supplemental

Supplemental related to this article can be found at http://dx.doi.org/10.1016/j.quascirev.2015.08.031.

References

Abbott, M.B., Edwards, M.E., Finney, B.P., 2010. A 40,000-yr record of environmental change from Burial Lake in Northwest Alaska. Quat. Res. 74, 156–165.
Abbott, M.B., Finney, B.P., Edwards, M.E., Kelts, K.E., 2000. Lake-level reconstructions and paleohydrology of Birch Lake, central Alaska, based on seismic reflection profiles and core transects. Quat. Res. 53, 154–166.
Abbott, M.B., Stafford, T.W., 1996. Radiocarbon geochemistry of modern and ancient

Arctic lake systems, Baffin Island, Canada. Quat. Res. 45, 300–311.
Ager, T.A., 2003. Late Quaternary vegetation and climate history of the central Bering land bridge from St. Michael Island, western Alaska. Quat. Res. 60, 19–32.
Amundson, R., Austin, A.T., Schuur, E.A.G., Yoo, K., Matzek, V., Kendall, C., Uebersax, A., Brenner, D., Baisden, W.T., 2003. Global patters of the isotopic composition of soil and plant nitrogen. Glob. Biogeochem. Cycles 17, 1031.
Anderson, P.M., 1985. Late Quaternary vegetational change in the Kotzebue Sound area, northwestern Alaska. Quat. Res. 24, 307–321.
Anderson, P.M., 1988. Late Quaternary pollen records from the Kobuk and Noatak River drainages, northwestern. Quat. Res. 29, 263–276.
Anderson, P.M., Brubaker, L.B., 1994. Vegetation history of northcentral Alaska: a mapped summary of late-Quaternary pollen data. Quat. Sci. Rev. 41, 306–315.
Anderson, P.M., Lozhkin, A.V., 2001. The Stage 3 interstadial complex (Karginskii/middle Wisconsinan interval) of Beringia: variations in paleoenvironments and implications for paleoclimatic interpretations. Quat. Sci. Rev. 20, 93–125.
Andresen, C.G., Lougheed, V.L., 2015. Disappearing Arctic tundra ponds: fine-scale analysis of surface hydrology in drained thaw lake basins over a 65year period (1948-2013). J. Geophys. Res. Biogeosci. 120, 466–479.
Badding, M.E., Briner, J.P., Kaufman, D.S., 2013. 10Be ages of late Pleistocene deglaciation and Neoglaciation in the north-central Brooks Range, Arctic Alaska. J. Quat. Sci. 28, 95–102.
Balser, A.W., Jones, J.B., Gens, R., 2014. Timing of retrogressive thaw slump initiation in the Noatak Basin, northwest Alaska, USA. J. Geophys. Res. Earth Surf. 119, 1106–1120.
Berger, A., Loutre, M.F., 1991. Insolation values for the climate of the last 10 million years. Quat. Sci. Rev. 10, 297–317.
Bieniek, P.A., Bhatt, U.S., Thoman, R.L., Angeloff, H., Partain, J., Papineau, J., Fritsch, F., Holloway, E., Walsh, J.E., Daly, C., Shulski, M., Hufford, G., Hill, D.F., Calos, S., Gens, R., 2012. Climate divisions for Alaska based on objective methods. J. Appl. Meteorol. Climatol. 51, 1276–1289.
Blaauw, M., 2010. Methods and code for 'classical' age-modelling of radiocarbon sequences. Quat. Geochronol. 5, 512–518.
Bond, G., Kromer, B., Beer, J., Muscheler, R., Evans, M.N., Showers, W., Hoffmann, S., Lotti-Bond, R., Hajdas, I., Bonani, G., 2001. Persistent solar influence on north Atlantic climate during the Holocene. Science 294, 2130–2136.
Briner, J.P., Kaufman, D.S., 2008. Late Pleistocene mountain glaciation in Alaska: key chronologies. J. Quat. Sci. 23, 659–670.
Brown, E.T., Johnson, T.C., Scholz, C.A., Cohen, A.S., King, J.W., 2007. Abrupt change in tropical African climate linked to the bipolar seesaw over the past 55,000 years. Geophys. Res. Lett. 34.
Caissie, B.E., Brigham-Grette, J., Lawrence, K.T., Herbert, T.D., Cook, M.S., 2010. Last Glacial Maximum to Holocene sea surface conditions at Umnak Plateau, Bering Sea, as inferred from diatom, alkenone, and stable isotope records. Paleoceanography 25.
Clark, P.U., Dyke, A.S., Shakun, J.D., Carlson, A.E., Clark, J., Wohlfarth, B., Mitrovica, J.X., Hostetler, S.W., McCabe, A.M., 2009. The Last Glacial Maximum. Science 325, 710–714.
Craine, J.M., Elmore, A.J., Aidar, M.P.M., Bustamante, M., Dawson, T.E., Hobbie, E.A., Kahmen, A., Mack, M.C., McLauchlan, K.K., Michelsen, A., Nardoto, G.B., Pardo, L.H., Penuelas, J., Reich, P.B., Schuur, E.A.G., Stock, W.D., Templer, P.H., Virginia, R.A., Welker, J.M., Wright, I.J., 2009. Global patterns of foliar nitrogen isotopes and their relationships with climate, mycorrhizal fungi, foliar nutrient concentrations, and nitrogen availability. New Phytol. 183, 980–992.
Croudace, I.W., Rindby, A., Rothwell, R.G., 2006. ITRAX: Description and Evaluation of a New Multi-function X-ray Core Scanner. New Techniques in Sediment Core Analysis. Geological Society, London Special Publications 267, pp. 51–63.
Darby, D.A., Ortiz, J.D., Grosch, C.E., Lund, S.P., 2012. 1,500-year cycle in the Arctic Oscillation identified in Holocene Arctic sea-ice drift. Nat. Geosci. 5, 897–900.
Dorfman, J.M., Stoner, J.S., Finkenbinder, M.S., Abbott, M.B., Xuan, C., St-Onge, G., 2015. A 37,000-yr environmental magnetic record of Aeolian dust deposition from Burial Lake, Arctic Alaska. Quat. Sci. Rev. (in this issue).
Dyke, A., 2004. An outline of the deglaciation of North America with emphasis on central and northern Canada. In: Ehlers, J., Gibbard, P.L. (Eds.), Quaternary Glaciations, Extent and Chronology. Part II. North America. Elsevier, Amsterdam.
Eisner, W.R., Colinvaux, P.A., 1992. Late Quaternary pollen records from Oil Lake and Feniak Lake, Alaska, U.S.A. Arct. Alp. Res. 24, 56–63.
Elias, S.A., 2000. Late Pleistocene climates of Beringia, based on analysis of fossil beetles. Quat. Res. 53, 229–235.
Elias, S.A., Hamilton, T.D., Edwards, M.E., Beget, J.E., Krumhardt, A.P., Lavoie, C., 1999. Late Pleistocene environments of the western Noatak basin, northwestern Alaska. Geol. Soc. Am. Bull. 111, 769–789.
Elias, S.A., Short, S.K., Nelson, C.H., Birks, H.H., 1996. Life and times of the Bering land bridge. Nature 382, 60–63.
Finkenbinder, M.S., Abbott, M.B., Edwards, M.E., Langdon, C.T., Steinman, B.A., Finney, B.P., 2014. A 31,000 year record of paleoenvironmental and lake-level change from Harding Lake, Alaska, USA. Quat. Sci. Rev. 87, 98–113.
Finney, B.P., Bigelow, N.H., Barber, V.A., Edwards, M.E., 2012. Holocene climate change and carbon cycling in a groundwater-fed, boreal forest lake: Dune Lake, Alaska. J. Paleolimnol. 48, 43–54.
Gaglioti, B.V., Mann, D.H., Jones, B.M., Pohlman, J.W., Kunz, M.L., Wooller, M.J., 2014. Radiocarbon age-offsets in an arctic lake reveal the long-term response of permafrost carbon to climate change. J. Geophys. Res. Biogeosci. 119, 1630–1651.
Grybeck, D., Beikman, H.M., Brosge, W.P., Tailleur, I.L., Mull, C.G., 1977. Geologic Map of the Brooks Range, Alaska, U.S. Geological Survey Open File Map of 77–166B. U.S. Geological Survey.
Guthrie, D.A., 2001. Origin and causes of the mammoth steppe: a story of cloud cover, woolly mammal tooth pits, buckles, and inside-out Beringia. Quat. Sci. Rev. 20, 549–574.
Hamilton, T.D., 1982. A late Pleistocene glacial chronology for the southern Brooks Range: stratigraphic record and regional significance. Geol. Soc. Am. Bull. 93, 700–716.
Hamilton, T.D., 2001. Quaternary glacial, lacustrine, and fluvial interactions in the western Noatak basin, Northwest Alaska. Quat. Sci. Rev. 20, 371–391.
Hamilton, T.D., 2003a. Surficial Geologic Map of Parts of the Misheguk Mountain and Baird Mountains Quadrangles, Noatak National Preserve, Alaska. U.S. Geological Survey Open File Report 03–367. U.S. Geological Survey.
Hamilton, T.D., 2003b. Surficial Geology of the Dalton High (Itkillik-Sagavanirktop Rivers) Area, Southern Arctic Foothills, Alaska. Professional Report 121. Alaska Division of Geological and Geophysical Surveys, p. 32.
Hamilton, T.D., 2010. Surficial Geologic Map of the Noatak National Preserve, Alaska. U.S. Geological Survey Scientific Investigations Map 3036. U.S. Geological Survey.
Hamilton, T.D., Lancaster, G.A., Trimble, D.A., 1987. Glacial advance of late Wisconsin (Itkillik II) age in the upper Noatak River valley—a radiocarbon-dated stratigraphic record. In: Survey, U.S.G. (Ed.), Geologic Studies in Alaska by the U.S. Geological Survey during 1986, pp. 35–39.
Hamilton, T.D., Van Etten, D.P., 1984. Late Pleistocene Glacial Dams in the Noatak Valley, The United States Geological Survey in Alaska -Accomplishments During 1981: U.S. Geological Survey Circular 868. U.S. Geological Survey, pp. 21–23.
Hartman, B., Wendler, G., 2005. The significance of the 1976 Pacific climate shift in the climatology of Alaska. J. Clim. 18, 4824–4839.
Heiri, O., Lotter, A.F., Lemcke, G., 2001. Loss on ignition as a method for estimating organic and carbonate content in sediments: reproducibility and comparability of results. J. Paleolimnol. 25, 101–110.
Higuera, P.E., Brubaker, L.B., Anderson, P.M., Hu, F.S., Brown, T.A., 2009. Vegetation mediated the impacts of postglacial climate change on fire regimes in the south-central Brooks Range, Alaska. Ecol. Monogr. 79, 201–219.
Hopkins, D.M., 1982. Aspects of the paleogeography of Beringia during the Late Pleistocene. In: Hopkins, D.M., Matthews, J.V., Schweger, C.E., Young, S.B. (Eds.), Paleoecology of Beringia. Academic Press, New York, pp. 3–28.
Hu, F.S., Finney, B.P., Brubaker, L.B., 2001. Effects of holocene Alnus expansion on aquatic productivity, nitrogen cycling, and soil development in southwestern Alaska. Ecosystems 4, 358–368.
Hu, F.S., Kaufman, D., Yoneji, S., Nelson, D., Shemesh, A., Huang, Y., Tian, J., Bond, G., Clegg, B., Brown, T., 2003. Cyclic variation and solar forcing of Holocene climate in the Alaskan subarctic. Science 301, 1890–1893.
Huybers, P., Wunsch, C., 2004. A depth-derived Pleistocene age model: uncertainty estimates, sedimentation variability, and nonlinear climate change. Paleoceanography 19.
Jones, M.C., Yu, Z., 2010. Rapid deglacial and early Holocene expansion of peatlands in Alaska. Proc. Natl. Acad. Sci. U. S. A. 107, 7347–7352.
Jorgenson, M.T., Yoshikawa, K., Kanveskiy, M., Shur, Y.L., Romanovsky, V., Marchenko, S., Grosse, G., Brown, J., Jones, B., 2008. Permafrost Characteristics of Alaska, Ninth International Conference on Permafrost. Alaska, Fairbanks, pp. 121–122.
Kaufman, D.S., Ager, T.A., Anderson, N.J., Anderson, P.M., Andrews, J.T., Bartlein, P.J., Brubaker, L.B., Coats, L.L., Cwynar, L.C., Duvall, M.L., Dyke, A.S., Edwards, M.E., Eisner, W.R., Gajewski, K., Geirsdottir, A., Hu, F.S., Jennings, A.E., Kaplan, M.R., Kerwin, M.N., Lozhkin, A.V., MacDonald, G.M., Miller, G.H., Mock, C.J., Oswald, W.W., Otto-Bliesner, B.L., Porinchu, D.F., Ruhland, K., Smol, J.P., Steig, E.J., Wolfe, B.B., 2004. Holocene thermal maximum in the western Arctic (0-180 degrees W). Quat. Sci. Rev. 23, 529–560.
Kaufman, D.S., Hu, F.S., Briner, J.P., Werner, A., Finney, B.P., Gregory-Eaves, I., 2003. A 33,000 year record of environmental change from Arolik Lake, Ahklun Mountains, Alaska, USA. J. Paleolimnol. 30, 343–362.
Keigwin, L.D., Donnelly, J.P., Cook, M.S., Driscoll, N.W., Brigham-Grette, J., 2006. Rapid sea-level rise and Holocene climate in the Chukchi Sea. Geology 34, 861–864.
Kling, G.W., Kipphut, G.W., Miller, M.C., 1991. Arctic lakes and rivers as gas conduits to the atmosphere: implications for tundra carbon budgets. Science 251, 298–301.
Kokorowski, H.D., Anderson, P.M., Mock, C.J., Lozhkin, A.V., 2008. A re-evaluation and spatial analysis of evidence for a Younger Dryas climatic reversal in Beringia. Quat. Sci. Rev. 27, 1710–1722.
Kurek, J., Cwynar, L.C., Ager, T.A., Abbott, M.B., Edwards, M.E., 2009. Late Quaternary paleoclimate of western Alaska inferred from fossil chironomids and it relation to vegetation histories. Quat. Sci. Rev. 28, 799–811.
Lewis, T., Gilbert, R., Lamoureux, S.F., 2002. Spatial and temporal changes in sedimentary processes at proglacial Bear Lake, Devon Island, Nunavut, Canada. Arct. Antarct. Alp. Res. 34, 119–129.
Mann, D.H., Groves, P., Reanier, R.E., Kunz, M.L., 2010. Floodplains, permafrost, cottonwood trees, and peat: what happened the last time climate warmed suddenly in arctic Alaska? Quat. Sci. Rev. 29, 3812–3830.
Mann, D.H., Peteet, D.M., Reanier, R.E., Kunz, M.L., 2002. Responses of an arctic landscape to Lateglacial and early Holocene climatic changes: the importance of moisture. Quat. Sci. Rev. 21, 997–1021.
Marcott, S.A., Shakun, J.D., Clark, P.U., Mix, A.C., 2013. A reconstruction of regional and global temperature for the past 11,300 years. Science 339, 1198–1201.

Max, L., Riethdorf, J.-R., Tiedemann, R., Smirnova, M., Lembke-Jene, L., Fahl, K., Nuernberg, D., Matul, A., Mollenhauer, G., 2012. Sea surface temperature variability and sea-ice extent in the subarctic northwest Pacific during the past 15,000 years. Paleoceanography 27.

Meyer, H., Schirrmeister, L., Yoshikawa, K., Opel, T., Wetterich, S., Hubberten, H.-W., Brown, J., 2010. Permafrost evidence for severe winter cooling during the Younger Dryas in northern Alaska. Geophys. Res. Lett. 37.

Meyers, P.A., Ishiwatari, R., 1993. Lacustrine organic geochemistry - an overview of indicators of organic matter sources and diagenesis in lake sediments. Org. Geochem. 20, 867–900.

Meyers, P.A., Teranes, J.L., 2001. Sediment organic matter. In: Last, W.M., Smol, J.P. (Eds.), Tracking Environmental Changes Using Lake Sediments, Physical and Chemical Techniques, vol. II. Kluwer, Dordecht, pp. 239–269.

Mock, C.J., Bartlein, P.J., Anderson, P.M., 1998. Atmospheric circulation patterns and spatial climatic variations in Beringia. Int. J. Climatol. 18, 1085–1104.

Monnin, E., Indermuhle, A., Dallenbach, A., Fluckiger, J., Stauffer, B., Stocker, T.F., Raynaud, D., Barnola, J.M., 2001. Atmospheric CO2 concentrations over the Last Glacial Termination. Science 291, 112–114.

Mortlock, R.A., Froelich, P.N., 1989. A simple method for the rapid determination of biogenic opal in pelagic marine sediments. Deep-Sea Res. 35, 1415–1426.

Oswald, W.W., Anderson, P.M., Brown, T.A., Brubaker, L.B., Hu, F.S., Lozhkin, A.V., Tinner, W., Kaltenrieder, P., 2005. Effects of sample mass and macrofossil type on radiocarbon dating of arctic and boreal lake sediments. Holocene 15, 758–767.

Oswald, W.W., Brubaker, L.B., Anderson, P.M., 1999. Late Quaternary vegetational history of the Howard Pass area, northwestern Alaska. Can. J. Bot. 77, 570–581.

Papineau, J.M., 2001. Wintertime temperature anomalies in Alaska correlated with ENSO and PDO. Int. J. Climatol. 21, 1577–1592.

Reimer, P.J., Baillie, M.G.L., Bard, E., Bayliss, A., Beck, J.W., Blackwell, P.G., Ramsey, C.B., Buck, C.E., Burr, G.S., Edwards, R.L., Friedrich, M., Grootes, P.M., Guilderson, T.P., Hajdas, I., Heaton, T.J., Hogg, A.G., Hughen, K.A., Kaiser, K.F., Kromer, B., McCormac, F.G., Manning, S.W., Reimer, R.W., Richards, D.A., Southon, J.R., Talamo, S., Turney, C.S.M., van der Plicht, J., Weyhenmeye, C.E., 2009. IntCAL09 and Marine09 radiocarbon age calibration curves, 0-50,000 years CAL BP. Radiocarbon 51, 1111–1150.

Santos, G.M., Southon, J.R., Drenzek, N.J., Ziolkowski, L.A., Druffel, E., Xu, X., Zhang, D., Trumbore, S., Eglinton, T.I., Hughen, K.A., 2010. Blank assessment for ultra-small radiocarbon samples: chemical extraction and separation versus AMS. Radiocarbon 52, 1322–1335.

Schnurrenberger, D., Russell, J., Kelts, K., 2003. Classification of lacustrine sediments based on sedimentary components. J. Paleolimnol. 29, 141–154.

Smith, I.R., 2000. Diamictic sediments within high Arctic lake sediment cores: evidence for lake ice rafting along the lateral glacial margin. Sedimentology 47, 1157–1179.

Stansell, N.D., Abbott, M.B., Rull, V., Rodbell, D.T., Bezada, M., Montoya, E., 2010. Abrupt Younger Dryas cooling in the northern tropics recorded in lake sediments from the Venezuelan Andes. Earth Planet. Sci. Lett. 293, 154–163.

Streten, N.A., 1974. Some features of the summer climate of interior Alaska. Arctic 27, 272–286.

Surdu, C.M., Duguay, C.R., Brown, L.C., Prieto, D.F., 2014. Response of ice cover on shallow lakes of the North Slope of Alaska to contemporary climate conditions (1950-2011): radar remote-sensing and numerical modeling data analysis. Cryosphere 8, 167–180.

Swanson, D.K., 2010. Satellite Greenness Data Summary for the Arctic Inventory and Monitoring Network, 1990-2009. Department of the Interior, N.P.S, pp. 1–20.

Wahrhaftig, C., 1965. Physiographic Divisions of Alaska. U.S. Geological Survey Professional Paper 482, p. 52.

Walter, K.M., Edwards, M.E., Grosse, G., Zimov, S.A., Chapin III, F.S., 2007. Thermokarst lakes as a source of atmospheric CH4 during the last deglaciation. Science 318, 633–636.

Wendler, G., Moore, B., Galloway, K., 2014. Strong temperature increase and shrinking sea ice in Arctic Alaska. Open Atmos. Sci. J. 8, 7–15.